Tunable thermal conductivity of ternary alloy semiconductors from first-principles

Francisco De Santiago[1,2], Martí Raya-Moreno[3], Alvaro Miranda[2], Miguel Cruz-Irisson[2], Xavier Cartoixà[3] and Riccardo Rurali[1]

[1] Institut de Ciència de Materials de Barcelona (ICMAB–CSIC), Campus de Bellaterra, 08193 Bellaterra, Barcelona, Spain

[2] Instituto Politécnico Nacional, ESIME-Culhuacan, Ciudad de México, Mexico

[3] Departament d'Enginyeria Electrònica, Universitat Autònoma de Barcelona, 08193 Bellaterra, Barcelona, Spain

E-mail: `rrurali@icmab.es`

Abstract. We compute the thermal conductivity, κ, of five representative III-V ternary alloys –namely $In_xGa_{1-x}As$, $GaAs_{1-x}P_x$, $InAs_{1-x}Sb_x$, $GaAs_{1-x}N_x$, and $GaP_{1-x}N_x$– in the whole range of compositions, and in zincblende and wurtzite crystal phases, using a first-principles approach and solving the phonon Boltzmann transport equation beyond the relaxation time approximation. We discuss the tunability of the thermal conductivity with the composition of the alloy, reporting the steep decrease of the thermal conductivity, followed by a wide plateau and a steep increase common in systems with lattice disorder. We also test the approximation consisting in considering impurities at small vales of x as bare mass defects, neglecting their chemical identity, and discuss its validity.

Submitted to: *J. Phys. D: Appl. Phys.*

1. Introduction

Alloying is one of the conceptually most straightforward way to design materials with tailor-made properties. Simply put, in a binary alloy of the kind $A_{1-x}B_x$, many important properties can be tuned between those of material A and those of material B by controlling the composition, x. If A and B have the same crystal structure, for instance, the heuristic Vegard's law [1, 2] predicts that the lattice parameter of an arbitrary alloy of composition x is $a_{A_{1-x}B_x} = (1-x)a_A + xa_B$, the weighted average of the lattice parameters of the two constituent materials, a_A and a_B. Although deviation from this ideal linear behavior can be observed [3, 4], Vegard's law remains an effective tool to make quick and reliable predictions and, considering its empirical nature, performs well in many cases of practical interest [5–7]. This simple linear interpolation is sometimes slightly less accurate when it comes to electronic properties, such as the bandgap, and a second order *bowing* parameter needs to be introduced in the case [8]. Nevertheless, despite the fact that the trend is not linear, it is still true that by controlling the composition, the properties of the alloy can be tuned to be a mixture of those of the constituent materials. A similar reasoning can be translated to ternary alloys of the kind $A_xB_{1-x}C$ or AB_xC_{1-x}, where the composition of the cation or of the anion is tuned. The capabilities of such a materials-by-design approach become virtually endless in nanostructured semiconductors, such as nanowires [9–11], where electrical and optical properties on-demand can be obtained by simultaneously controlling two or more parameters among the composition, the growth direction, the diameter and, more recently, the crystal phase [12–17].

Importantly, the control of the composition of an alloy not only permits tuning the properties of the material itself, but can also be used to create lattice-matched heterojunctions that would otherwise be bedeviled by multiple defects arising to allow releasing the elastic strain that builds up at the interface. $In_xGa_{1-x}As$, for instance, which is an important material for high-speed photodetectors, can be grown epitaxially on InP when $x = 0.53$ [18, 19]. Similarly, while only three layers of Ge can be grown on a Si substrate before stacking faults develop, defect-free $Si/Si_{1-x}Ge_x$ interfaces can be obtained [11, 20].

The thermal transport properties of ternary alloys received much less attention, if compared to electronic and structural properties, and theoretical results are scarce, due to the difficulty to model disordered systems. Yet, alloys are expected to scatter efficiently phonons [21, 22] and can thus play an important role in the design of efficient thermoelectrics [23]. Indeed, narrow-gap semiconductor alloys are used in applications for both power generation and cooling, where the use of other means is not feasible or practical [24]. Criteria have been developed to predict whether the reduction in thermal conductivity due to alloying will be more beneficial than the ensuing reduction of electrical conductivity, thus leading to improved thermoelectric performance [25]. Much of our current understanding of the physical principle behind alloy scattering is due to Klemens [26], who obtained an expression for lattice thermal conductivity at high

temperatures, when scattering point defects is the dominating scattering mechanism. This pioneering model, nonetheless, rests on some simplifying assumptions that must be circumvented in order to attain quantitative predictions. In particular it assumes that point defects scatter in virtue of their mass difference and neglect their chemical identity. First-principles calculations, like those here presented, intend to overcome this limitation.

In this work we study the thermal conductivity of five III-V ternary alloys within a first-principles approach, computing the interatomic force constants from density-functional theory and then solving the phonon Boltzmann Transport Equation (BTE) beyond the Relaxation Time Approximation (RTA). We consider $In_xGa_{1-x}As$, $GaAs_{1-x}P_x$, and $InAs_{1-x}Sb_x$ as prototypical alloys that can be synthesized throughout the full range of compositions [5, 27–31], with $0 < x < 1$, and that feature a variable mixture of the cation ($In_xGa_{1-x}As$) and of the anion ($GaAs_{1-x}P_x$ and $InAs_{1-x}Sb_x$). $In_xGa_{1-x}As$ and $InAs_{1-x}Sb_x$ are important materials for photodetectors [18, 32], while $GaAs_{1-x}P_x$ is used in the manufacture of red, orange and yellow light-emitting diodes [33], and is important in crystal phase engineering, where both wurtzite and crystal phase superlattices nanowires have been reported [34,35]. Additionally, we study $GaAs_{1-x}N_x$ and $GaP_{1-x}N_x$, two diluted nitride semiconductors where spatially selective hydrogen irradiation can be used to design site-controlled quantum dots and nanowires and that find applications in optoelectronics and spintronics [36, 37].

Our approach, as discussed in more detail below, consists in describing the alloy as a virtual crystal with effective parameters derived from those of the constituent materials. Therefore, our results are valid for fully random alloys, where no local ordering or concentration gradients are important [38, 39]. In this sense, they are a generalization of the more simplified models used by Adachi [40, 41], Nakwaski [42], and Szmulowicz *et al.* [43] (Ref. 41 does consider ordering effects, but not for ternary semiconductors).

Despite the relatively crude approach, the description of random alloys in term of a virtual crystal has shown to yield good results. For instance, Li *et al.* [44] studied $Mg_2Si_xSn_{1-x}$, taking, in full analogy with our approach, the IFCs of the alloy as the average of those for the constituent materials and neglecting IFCs disorder. They obtain results in good agreement with experimental results [45–48] in a wide range of compositions. Similarly, the virtual crystal results obtained by Garg *et al.* [49] exhibit a very good agreement with previous experimental results as well [50, 51]. The effect of long-range order was explicitly addressed by Mei and Knezevic [52], who studied bulk ternary III-V arsenide alloys using molecular dynamics with an optimized Albe-Tersoff empirical interatomic potentials and provided a complementary and important insight on phonon scattering beyond the random-alloy assumption. Also, a conceptually interesting approach has been followed by Arrigoni *et al.* [53], who considered explicitly the disorder in the force constants and showed that in some cases, namely $In_xGa_{1-x}As$ which is also discussed in this work, it is necessary to attain a good agreement with the available experimental data. Although this method still cannot account for concentration gradients or non uniform alloy distributions, it has the benefit of relying

on fully first-principles data, yet going beyond the virtual crystal approximation where only mass disorder is considered.

2. Computational Methods

We performed density-functional theory (DFT) calculations, using the VASP [54] code with projector augmented-wave (PAW) method [55, 55] and the Local Density Approximation (LDA) for the exchange-correlation as parameterized by Perdew and Zunger [56] to Ceperley-Alder [57]. We sample the Brillouin zone with a converged $16 \times 16 \times 16$ shifted mesh and optimized the lattice parameter until stresses lower than $3 \cdot 10^{-3}$ GPa were attained (the forces are zero by symmetry). An additional density functional perturbation theory (DFPT) calculation, with a doubled k-mesh, was carried out to obtain the Born charges (Z^*) and dielectric constant at high frequency (ε^∞), needed to calculate the non-analytic term correction for the dynamical matrix near Γ. The harmonic and third-order anharmonic interatomic force constants (IFCs) were calculated by finite differences in a $5 \times 5 \times 5$ and a $4 \times 4 \times 4$ supercell, respectively, with the PHONOPY [58] and the THIRDORDER.PY [59] codes. We considered bulk zincblende crystals of GaP, GaAs, InAs, InSb, and GaN. The alloy is modeled as a virtual crystal with effective parameters obtained by averages of the kind $\Phi_{VC} = \sum_i x_i \Phi_i$, where x_i is the concentration of component i and Φ_i is the lattice parameter, an atomic coordinate, a harmonic or anharmonic IFC, the dielectric tensor or a Born effective charge. The compositional disorder of the alloy is treated as a random mass perturbation of the reference virtual crystal, in analogy to mass disorder scattering in a single crystal in the model due to Tamura [60] We also report results for selected alloys with the wurtzite crystal structure. In those cases the Brillouin zone is sampled with a $16 \times 16 \times 12$ mesh of **k**-points, structural relaxations are performed until all the forces are lower than 5×10^{-4} eV/AA and we used a $4 \times 4 \times 3$ supercell for both harmonic and anharmonic IFCs.

This approximate description of the alloy has the obvious advantage that, given the IFCs of two or more pure crystals are available, one can compute the thermal conductivity of all the alloys that can be constructed from them and in all the concentration range, without the need of performing additional DFT calculations. The main limitation of this approach is that it cannot account for local structural relaxation and that it assumes a uniform concentration. Whenever one of these factors is important, one must resort to different numerical approaches, such as classical molecular dynamics, where very large computational cells can be tackled and concentration gradients and local relaxation can be explicitly accounted for [52]. Typically, however, this means giving up on the predictive power of *ab initio* calculations. The assumption of random alloy, in particular, is challenged by X-ray and transmission electron microscopy experiments that show that, in some conditions, ternary alloys exhibit a certain order. This is the case of $Al_xGa_{1-x}As$ and $Al_xIn_{1-x}As$ (see Refs 61–65), not studied here, but also of $In_xGa_{1-x}As$(see Refs. 66–68).

Once the IFCs are obtained (either those of the pure crystal or those of the virtual crystal, i.e. the alloy), we use them to solve self-consistently the linearized Boltzmann Transport Equation (BTE) for phonons using the almaBTE code [69] and sampling the Brillouin zone with a $30 \times 30 \times 30$ and a $30 \times 30 \times 16$ grid of $\mathbf{q}$-points for the zincblende and the wurtzite, respectively. The lattice thermal conductivity tensor ($\kappa^{\alpha\beta}$) is obtained as:

$$\kappa^{\alpha\beta} = \frac{1}{Nk_B\Omega T^2} \sum_{\lambda} n_0(n_0+1)(\hbar\omega_\lambda)^2 v_\lambda^\alpha F_\lambda^\beta, \tag{1}$$

where α and β label the Cartesian axes x, y and z; N, k_B, Ω, T are the number of $\mathbf{q}$-points, the Boltzmann constant, the cell volume and the temperature, respectively. The summation is done over all phonon modes λ, which are characterized by the band label n and their $\mathbf{q}$-vector. n_0 is the equilibrium Bose-Einstein distribution function, $\hbar$ is the reduced Planck constant, ω_λ is the phonon mode frequency and v_λ^α is the group velocity of phonon mode λ along the α direction. F_λ^β is the generalized mean free path of the phonon mode along the β direction, and it is calculated as $\tau_\lambda(v_\lambda^\beta + \Delta_\lambda^\beta)$. τ_λ is the lifetime of the phonon in the relaxation time approximation (RTA) and Δ_λ^β is a measure of how much the population of a specific phonon mode and its associated heat current deviates from the RTA prediction [59]. This correction is obtained iteratively starting from the RTA ($\Delta_\lambda^\beta = 0$).

Scattering from isotopic disorder, besides anharmonic three-phonon scattering, is also included considering the natural isotopic distributions of the elements involved through the model of Tamura [60].

3. Results and Discussion

Figure 1 displays the main results of our study: the thermal conductivity of the five alloy compounds investigated throughout all the composition range and at three representative temperatures: 100, 300, and 500 K. All of them exhibit a U-shaped dependence of κ as a function of the composition, which is common to other systems featuring some kind of disorder in the crystal lattice, in the form of point or extended defects, such as in binary SiGe alloys [49], isotope disorder [70] and porous Si [71, 72] and has been reported in experimental studies of ternary alloys [40, 42, 50, 73–81]. It consists of a very steep descent at low values of x, followed by an extended plateau and a similarly steep increase as x approaches 1. This behavior indicates that the fluctuation of the composition results in efficient scattering, causing a reduction of the phonon mean free path. This reduction stems from the fact that a relatively small number of scatterers is sufficient to yield a large decrease in the thermal conductivity, so that additional scatterers have little effect, as they cannot reduce κ much further. The interest in this kind of $\kappa(x)$ dependence is two-fold: (i) if one wants to design a low thermal conductivity material for thermoelectric applications, a relatively low level of alloying (i.e. a small concentration of *impurities*) is needed; (ii) in a wide range of compositions the thermal conductivity has a weak dependence on the exact value of

x and thus makes easier the task of designing a material with a given κ. The width of the low κ central plateau is estimated in Table 1, where we assume to be in the extreme alloying limit when the thermal conductivity is at most 10% larger than its minimum value. Typically, this region becomes larger at higher temperature. This is a result of the increased anharmonic scattering that tends to smooth the $\kappa(x)$ curves (it has a comparatively larger effect on those compositions where disorder induced scattering is lower). Also, Table 1 highlights the fact that $\kappa(x)$ is not, in general symmetric, and the low conductivity plateau is not centered around 0.5, something already visible in Figure 1. Because of the importance of very low N content in diluted nitrides for applications in spintronics and optoelectronics, we show a zoomed view of the $0 < x < 0.1$ region in $GaAs_{1-x}N_x$ and $GaP_{1-x}N_x$, as insets of the corresponding panels of Figure 1. These magnified views further emphasize the steep dependence of the thermal conductivity on the composition, so that, for instance, a bare 2% of N content in $GaAs_{1-x}N_x$ at room temperature reduces κ to half the value of GaAs, the reference pure compound. This behavior is common to all five materials and is summarized in Figure 2. As it can be seen there, less than 10% of lattice defects yields most of the total reduction of the thermal conductivity in all cases. It is also interesting to stress again that, in a given compound, the behavior is not symmetric. Therefore, if one focuses on $GaAs_{1-x}P_x$, it is easy to see that small quantities of As are much more effective in reducing the thermal conductivity of GaP than similar amounts of P atoms are in reducing the thermal conductivity of GaAs (compare for instance the case of $GaAs_{0.8}P_{0.2}$ and $GaAs_{0.2}P_{0.8}$ on the left-hand side and right-hand side panel of Figure 2). Similar observations can be made for the other materials, with the exception of $In_xGa_{1-x}As$ where alloying InAs with Ga has similar effects of alloying GaAs with In.

Substitutional defects induce a rather localized lattice distortion and thus they are expected to scatter mostly short wavelength, high frequency phonons. For this reason, it has been previously suggested that isotopical lattice disorder results in a low-pass filtering effect [70, 82]. Additionally, within the approach used here, defects are treated as random mass perturbations of the reference virtual crystal and local relaxations are neglected, i.e. the lattice distortion mentioned above has no spatial extension and collapses at the impurity sites [60]. This means that we are probably overestimating the cutoff frequency and, within a more realistic (but computationally unaffordable at the first-principles level) model that accounts for local relaxations, also phonons of somewhat lower frequencies would be scattered.

This behavior is indeed captured by the frequency resolved thermal conductivity, $\kappa(\omega)$, shown in Figure 3. However, these results reveal a more nuanced scenario. As it can be seen in the case of GaAs, low frequency, long wavelength acoustic phonons with $f < 1.75$ THz are not affected by small contents of P or N, and the $\kappa(\omega)$ of pristine GaAs is recovered. In agreement with the simple low-pass filter model described above, at higher frequencies acoustic phonons start to be scattered. This happens because, due to their fairly linear dispersion, high frequency acoustic phonons have short wavelength and thus interact with localized lattice distortion. If we move further up in frequency,

however, this simple rule breaks down and high frequency (4 THz $< f <$ 6 THz) acoustic phonons next to zone boundaries, which would be expected to be strongly scattered in view of their short wavelength, exhibit an almost perfect transmission. Notice that in this frequency range only longitudinal acoustic (LA) phonons are present [see the dispersion relation of pristine GaAs in the left hand side of Figure 3(a)]. This trend is confirmed by the results of Figure 3(b), which refer to GaP in presence of small amounts of As or N (and where the situation is even clearer due to a well-defined acoustic-optical gap). Also in this case, phonons with frequencies between 4 and 7 THz suffer negligible scattering, highlighting a fundamental difference between transverse acoustic (TA) and LA phonons. While the former obey the simple rule that only short wavelength phonons are scattered, the latter are essentially unaffected by the alloy disorder. The behavior of optical phonons is more subtle, as it is more difficult to draw a connection between wavelength and frequency. For instance the lowest lying optical phonon along the K-Γ direction has a smaller frequency close to the zone boundary, where stronger scattering is expected, than at the zone center. More in general, optical phonons tend to have rather flat dispersion, so that the two protypical patterns outlined above –short wavelength, strong scattering / long wavelength, low scattering– are often mixed. Indeed, the whole optical band of GaAs seems to undergo a uniform scattering in line with these observations (in the case of GaP the contribution of optical phonons is so small that is difficult to say something conclusive). Therefore, differently from the most common strategies to reduce the thermal conductivity of a material, which rely on the increased scattering of long wavelength phonons, in alloys the decrease of κ derives from the enhanced scattering of high frequency TA phonons and optical phonons, though the contribution of the latter is smaller. These results agree with previous reports of isotope disorder [70, 82] and binary alloys [83] and indicate that substitutional mass defects can be used to design phonon low-pass filter that mostly suppress midrange and high frequencies phonons. Nevertheless, our results indicate that LA phonons, regardless of their frequency, are not scattered and can originate a mid frequency pass band, between the TA and the optical bands.

Up to this point we have related more than once alloying with isotope disorder. The reason is that, in all the alloys considered, we have replaced a fraction of group-III with a different type of group-III atom (Ga and In) or fraction of group-V with a different type of group-V atom (As and P, As and Sb, and the diluted nitrides), so that the bonding arrangement is preserved. Therefore, to a first approximation, one might expect that the additional scattering comes mostly from the mass difference and that the chemical identities of the atoms involved in the alloying play a minor role. To verify the validity of this picture, we have calculated the thermal conductivity of $InAs_{1-x}Sb_x$ and $GaAs_{1-x}N_x$ where, rather than relying on the IFCs of the virtual crystal, which are obtained mixing those of InAs and InSb and those of GaAs and GaN, we have designed isotope populations where a fraction x of As atoms have the mass of Sb in one case and N in the other. In this way we treat Sb and N atoms as *heavy* and *light* As atoms, respectively. Validating this simple approximation could be important for large-scale

molecular dynamics calculations, suitable to account for non-uniform compositions or nanostructuring, where typically classical interatomic potential of III-V material exist, but are not available for the multiple possible ternary alloys. As can be seen in Figure 4, in the case of $GaAs_{1-x}N_x$ the predictions of the mass defect model are in reasonable agreement with the results obtained with the virtual crystal. The differences tend to vanish at low concentrations and high temperatures, with the latter factor playing a more important role. These results suggest that molecular dynamics simulations –that are normally carried out at high temperature, where the approximation of classical atomic trajectories is justified– can be performed with a reliable interatomic potential for GaAs, modeling N atoms as mass defects. On the other hand, the performance of the mass defect model is significantly worse in the case of $InAs_{1-x}Sb_x$, where even at room temperature the discrepancy with the virtual crystal is considerable. It would be tempting to speculate that the different accuracy of the mass defect model stems from the difference in mass ratios. One could expect that in the case of large mass ratios, e.g. $m_{As}/m_N \sim 5$, much of the scattering comes from the difference in the masses involved and thus approximating the minority element as a mass defect should yield reasonable results. Conversely, when masses are in the same range, e.g. $m_{As}/m_{Sb} \sim 0.6$, the chemical identity of the impurities will have a more important role in determining phonon scattering and the mass defect model should not perform too well; the limiting case would be a mass ratio of 1, where the mass defect approximation would predict no alloy scattering. This qualitative picture, however, is only partially supported by our data. For instance, the accuracy of the mass defect model in $GaAs_{1-x}N_x$ is quite different at low values of x, where small concentrations of N scatters phonons on GaAs and at high values of x, where the situation is reversed and As impurities scatter phonons of GaN. The mass ratio is obviously the same, but the prediction of the mass defect model are closer to the results of the virtual crystal for low values of N content. These results suggest that, while sometimes the simple mass defect model can perform quite well, it is difficult to know it in advance and its accuracy should be validated case by case.

When ternary III-V alloys are grown in the form of nanowires (NWs), other structural parameters, such as the diameter or the crystallographic orientation, can be used together with the composition to design materials with tailor-made properties. Several reports of $InAs_{1-x}Sb_x$ NWs have been published, both as pure wires [84–86] or as part of axial heterojunctions [87,88], in a wide range of compositions; $In_xGa_{1-x}As$ NWs have been reported as well, either as stand-alone NW [89] or as shell material in core-shell NWs [90,91]; diluted nitrides have become available only recently in NW geometry, but it is a field in rapid expansion for its applications in nanoscale photonics (see Ref. 92 and references therein). Remarkably, it is possible to synthesize NWs in crystal phases that in the bulk can only be obtained in extreme conditions of temperature and/or pressure and this applies also to alloys, thus adding more flexibility in the design of materials with desired properties. For instance, wurtzite $In_xGa_{1-x}As$ NWs [90, 93], $GaAs_{1-x}P_x$ NWs [34] and $GaAs_{1-x}P_x$ crystal phase superlattices [35] –where different polytypes of

the same material, rather than different materials are alternated in a periodic manner– have all been reported. This is remarkable, as both InAs, GaAs, and GaP are cubic zincblende crystal in the bulk, at room temperature and atmospheric pressure. Because of the relevance of this *so-called* crystal phase engineering in NWs, we have also studied the five alloys discussed above when they take the wurtzite crystal phase. We found that the behavior of the thermal conductivity as a function of the composition and the underlying physics are the same of the cubic polytypes and the existing differences stem from the different overall anharmonicity of the constituent materials [94]. This similarity can be appreciated in Figure 5, where we plot $\kappa(x)$ of wurtzite $In_xGa_{1-x}As$ and $GaAs_{1-x}P_x$. The only noticeable difference with the zincblende is, of course, that in the wurtzite the thermal conductivity tensor is no longer isotropic as it was in the cubic lattice and we thus distinguish between its two independent components, $\kappa_{xx} = \kappa_{yy}$ and κ_{zz}. As it can be seen, κ of the zincblende (which we plot for $T = 100$ K) is almost indistinguishable from κ_{xx} of the wurtzite at practically all the concentrations studied. This is an important observation, because the thermal conductivity of the pure materials do differ between the two polytypes, as discussed at length by some us in Ref. 94. Therefore, alloying tends to erase this difference, at least concerning the comparison of the isotropic κ of the zincblende with κ_{xx} of the wurtzite. For instance, for GaAs at 300 K we obtain a thermal conductivity of 47.2 and 39 W m^{-1} K^{-1} for the zincblende and the wurtzite in the xy-plane, yielding a ratio $\kappa^{GaAs,ZB}/\kappa^{GaAs,WZ}_{xx} = 1.21$. Similarly, we find $\kappa^{InAs,ZB}/\kappa^{InAs,WZ}_{xx} = 1.11$. However, $\kappa^{In_xGa_{1-x}As,ZB}/\kappa^{In_xGa_{1-x}As,WZ}_{xx}$ takes values between 0.99 and 1.01 for $0.4 < x < 0.9$.

4. Conclusions

We have presented first-principles calculations based on a virtual crystal approach of the thermal conductivity of five representative III-V alloys throughout the whole concentration range, x. We found that, similar to other systems characterized by some degree of disorder of the crystal lattice, the thermal conductivity features a strong dependence on the composition at small and high vales of x, with a wide plateau in the central region. The reduction of the thermal conductivity derives from the increased scattering experienced by high frequency transverse acoustic phonons and optical phonons. We also discussed to what extent a simple mass defect model can be employed to yield reliable predictions, but found that its accuracy is strongly system-dependent.

Acknowledgments

We acknowledge financial support by the Ministerio de Economía, Industria y Competitividad (MINECO) under grant FEDER-MAT2017-90024-P and the Severo Ochoa Centres of Excellence Program under Grant SEV-2015-0496, the Ministerio de Ciencia, Innovación y Universidades under Grant No. RTI2018-097876-B-C21

(MCIU/AEI/FEDER, UE), and by the Generalitat de Catalunya under grants no. 2017 SGR 1506. MRM is supported by the Ministerio de Educación, Cultura y Deporte through the program of Formación de Profesorado Universitario under Grant No.FPU2016/02565. AM and MCI acknowledge financial support through the multidisciplinary project IPN-SIP 2020-2093. FDS acknowledges financial support from scholarships CONACYT-Movilidad and BEIFI-IPN. We thank the Centro de Supercomputación de Galicia (CESGA) for the use of their computational resources. RR thanks Marta De Luca for useful discussions.

[1] Denton A R and Ashcroft N W 1991 *Phys. Rev. A* **43**(6) 3161–3164
[2] Jacob K T, Raj S and Rannesh L 2007 *Int. J. Mater. Res.* **98**(9) 776–779
[3] Bellaiche L, Wei S H and Zunger A 1996 *Phys. Rev. B* **54**(24) 17568–17576
[4] Murphy S T, Chroneos A, Jiang C, Schwingenschlögl U and Grimes R W 2010 *Phys. Rev. B* **82**(7) 073201
[5] Nahory R E, Pollack M A, Johnston W D and Barns R L 1978 *Appl. Phys. Lett.* **33** 659–661
[6] Iori F, Ossicini S and Rurali R 2014 *J. Appl. Phys.* **116** 154301
[7] Cartoixà X, Palummo M, Hauge H I T, Bakkers E P A M and Rurali R 2017 *Nano Lett.* **17** 4753–4758
[8] Vurgaftman I, Meyer J R and Ram-Mohan L R 2001 *J. Appl. Phys.* **89** 5815–5875
[9] Lu W and Lieber C M 2006 *J. Phys. D: Appl. Phys.* **39** R387–R406
[10] Rurali R 2010 *Rev. Mod. Phys.* **82** 427–449
[11] Amato M, Palummo M, Rurali R and Ossicini S 2014 *Chem. Rev.* **114** 1371–1412
[12] Caroff P, Dick K A, Johansson J, Messing M E, Deppert K and Samuelson L 2009 *Nat. Nanotech.* **4** 50–55
[13] Dick K A, Thelander C, Samuelson L and Caroff P 2010 *Nano Lett.* **10** 3494–3499
[14] Caroff P, Bolinsson J and Johansson J 2011 *IEEE Journal of Selected Topics in Quantum Electronics* **17** 829–846
[15] Jacobsson D, Panciera F, Tersoff J, Reuter M C, Lehmann S, Hofmann S, Dick K A and Ross F M 2016 *Nature* **531** 317–322
[16] Amato M, Kaewmaraya T, Zobelli A, Palummo M and Rurali R 2016 *Nano Lett.* **16** 5694–5700
[17] Raya-Moreno M, Aramberri H, Seijas-Bellido J A, Cartoixà X and Rurali R 2017 *Appl. Phys. Lett.* **111** 032107
[18] Takeda Y, Sasaki A, Imamura Y and Takagi T 1976 *J. Appl. Phys.* **47** 5405–5408
[19] Pearsall T 1980 *IEEE Journal of Quantum Electronics* **16** 709–720
[20] David T, Aqua J N, Liu K, Favre L, Ronda A, Abbarchi M, Claude J B and Berbezier I 2018 *Sci. Rep.* **8** 2891
[21] Giri A, Braun J L, Rost C M and Hopkins P E 2017 *Scr. Mater.* **138** 134 – 138
[22] Gurunathan R, Hanus R and Snyder G J 2020 *Mater. Horiz.* **7**(6) 1452–1456
[23] Benenti G, Casati G, Saito K and Whitney R S 2017 *Physics Reports* **694** 1–124
[24] Shakouri A 2011 *Annu. Rev. Mater. Res.* **41** 399–431
[25] Wang H, LaLonde A D, Pei Y and Snyder G J 2013 *Adv. Funct. Mater.* **23** 1586–1596
[26] Klemens P G 1960 *Phys. Rev.* **119**(2) 507–509
[27] Snyder C W, Orr B G, Kessler D and Sander L M 1991 *Phys. Rev. Lett.* **66**(23) 3032–3035
[28] Svensson S P, Sarney W L, Hier H, Lin Y, Wang D, Donetsky D, Shterengas L, Kipshidze G and Belenky G 2012 *Phys. Rev. B* **86**(24) 245205
[29] Lee G S, Lo Y, Lin Y F, Bedair S M and Laidig W D 1985 *Appl. Phys. Lett.* **47** 1219–1221
[30] Jen H R, Cao D S and Stringfellow G B 1989 *Appl. Phys. Lett.* **54** 1890–1892
[31] Geisz J F, Olson J M, Romero M J, s Jiang C and Norman A G 2006 *2006 IEEE 4th World Conference on Photovoltaic Energy Conference* vol 1 pp 772–775
[32] Rogalski A, Martyniuk P, Kopytko M, Madejczyk P and Krishna S 2020 *Sensors* **20** 7047
[33] Zhu D and Humphreys C J 2016 *Solid-State Lighting Based on Light Emitting Diode Technology* (Cham: Springer International Publishing) pp 87–118
[34] Assali S, Zardo I, Plissard S, Kriegner D, Verheijen M A, Bauer G, Meijerink A, Belabbes A, Bechstedt F, Haverkort J E M and Bakkers E P A M 2013 *Nano Lett.* **13** 1559–1563
[35] Dick K A, Deppert K, Larsson M W, Mårtensson T, Seifert W, Wallenberg L R and Samuelson L 2004 *Nat. Mater.* **3** 380–384
[36] Biccari F, Boschetti A, Pettinari G, La China F, Gurioli M, Intonti F, Vinattieri A, Sharma M, Capizzi M, Gerardino A, Businaro L, Hopkinson M, Polimeni A and Felici M 2018 *Adv. Mater.* **30** 1705450
[37] Felici M, Pettinari G, Biccari F, Capizzi M and Polimeni A 2018 *Semicond. Sci. Technol.* **33**

053001
[38] Lindsay L, Katre A, Cepellotti A and Mingo N 2019 *J. Appl. Phys.* **126** 050902
[39] Seyf H R, Yates L, Bougher T L, Graham S, Cola B A, Detchprohm T, Ji M H, Kim J, Dupuis R, Lv W and Henry A 2017 *npj Computational Materials* **3** 49
[40] Adachi S 1983 *J. Appl. Phys.* **54** 1844–1848
[41] Adachi S 2007 *J. Appl. Phys.* **102** 063502
[42] Nakwaski W 1988 *J. Appl. Phys.* **64** 159–166
[43] Szmulowicz F, Madarasz F L, Klemens P G and Diller J 1989 *J. Appl. Phys.* **66** 252–255
[44] Li W, Lindsay L, Broido D A, Stewart D A and Mingo N 2012 *Phys. Rev. B* **86**(17) 174307
[45] Rowe D M 2005 *Thermoelectrics Handbook* (Taylor & Francis)
[46] Zhang Q, He J, Zhu T J, Zhang S N, Zhao X B and Tritt T M 2008 *Appl. Phys. Lett.* **93** 102109
[47] Chen H Y, Savvides N, Dasgupta T, Stiewe C and Mueller E 2010 *phys. stat. sol. (a)* **207** 2523–2531
[48] ichi Tani J and Kido H 2005 *Physica B* **364** 218–224
[49] Garg J, Bonini N, Kozinsky B and Marzari N 2011 *Phys. Rev. Lett.* **106**(4) 045901
[50] Abeles B 1963 *Phys. Rev.* **131**(5) 1906–1911
[51] Stohr H and Klemm W 1954 *Z. Anorg. Allg. Chem.* **241** 304
[52] Mei S and Knezevic I 2018 *J. Appl. Phys.* **123** 125103
[53] Arrigoni M, Carrete J, Mingo N and Madsen G K H 2018 *Phys. Rev. B* **98**(11) 115205
[54] Kresse G and Furthmüller J 1996 *Phys. Rev. B* **54** 11169
[55] Kresse G and Joubert D 1999 *Phys. Rev. B* **59** 1758
[56] Perdew J P and Zunger A 1981 *Phys. Rev. B* **23**(10) 5048–5079
[57] Ceperley D M and Alder B J 1980 *Phys. Rev. Lett.* **45**(7) 566–569
[58] Togo A and Tanaka I 2015 *Scr. Mater.* **108** 1–5
[59] Li W, Carrete J, Katcho N A and Mingo N 2014 *Comp. Phys. Commun.* **185** 1747–1758
[60] Tamura S 1983 *Phys. Rev. B* **27**(2) 858–866
[61] Kuan T S, Kuech T F, Wang W I and Wilkie E L 1985 *Phys. Rev. Lett.* **54** 201
[62] Gomyo A, Makita K, Hino I and Suzuki T 1994 *Phys. Rev. Lett.* **72** 673
[63] Suzuki T, Ichihashi T and Nakayama T 1998 *Appl. Phys. Lett.* **73** 2588
[64] Forrest R L, Kulik J, Golding T D and Moss S C 2000 *J. Mater. Res.* **15** 45
[65] Ohkouchi S, Furuhashi T, Gomyo A, Makita K and Suzuki T 2005 *Appl. Surf. Sci.* **241** 9
[66] Kuan T S, Wang W I and Wilkie E L 1987 *Appl. Phys. Lett.* **51** 51
[67] Mori T, Hanada T, Morimura T, Shin K, Makino H and Yao T 2004 *Appl. Surf. Sci.* **237** 230
[68] Shin K, Yoo J, Joo S, Mori T, Shindo D, Hanada T, Makino H, Cho M, Yao T and Park Y G 2006 *Mater. Trans.* **47** 1115
[69] Carrete J, Vermeersch B, Katre A, van Roekeghem A, Wang T, Madsen G K and Mingo N 2017 *Comput. Phys. Commun.* **220** 351–362
[70] Royo M and Rurali R 2016 *Phys. Chem. Chem. Phys.* **18**(37) 26262–26267
[71] Dettori R, Melis C, Cartoixà X, Rurali R and Colombo L 2015 *Phys. Rev. B* **91**(5) 054305
[72] Cartoixà X, Dettori R, Melis C, Colombo L and Rurali R 2016 *Appl. Phys. Lett.* **109**(1) 013107
[73] Abrahams M, Braunstein R and Rosi F 1959 *Journal of Physics and Chemistry of Solids* **10** 204–210
[74] Carlson R O, Slack G A and Silverman S J 1965 *J. Appl. Phys.* **36** 505–507
[75] Afromowitz M A 1973 *J. Appl. Phys.* **44** 1292–1294
[76] Ohmer M C, Mitchel W C, Graves G A, Holmes D E, Kuwamoto H and Yu P W 1988 *J. Appl. Phys.* **64** 2775–2777
[77] Arasly D G, Ragimov R N and Aliev M I 1990 *Sov. Phys. Semicond.* **24** 225
[78] Magomedov Y B, Kramynina N L and Ismaílov S M 1992 *Soviet physics. Solid state.* **34** 1486
[79] Pichardo J L, Alvarado-Gil J J, Cruz A, Mendoza J G and Torres G 2000 *J. Appl. Phys.* **87** 7740–7744
[80] Daly B C, Maris H J, Nurmikko A V, Kuball M and Han J 2002 *J. Appl. Phys.* **92** 3820–3824
[81] Liu W and Balandin A A 2004 *Applied Physics Letters* **85** 5230–5232

[82] Stewart D A, Savić I and Mingo N 2009 *Nano Lett.* **9** 81–84
[83] Xiong S, Sääskilahti K, Kosevich Y A, Han H, Donadio D and Volz S 2016 *Phys. Rev. Lett.* **117**(2) 025503
[84] Potts H, Friedl M, Amaduzzi F, Tang K, Tütüncüoglu G, Matteini F, Alarcon Lladó E, McIntyre P C and Fontcuberta i Morral A 2016 *Nano Lett.* **16** 637–643
[85] Namazi L, Ghalamestani S G, Lehmann S, Zamani R R and Dick K A 2017 *Nanotechnology* **28** 165601
[86] Boland J L, Amaduzzi F, Sterzl S, Potts H, Herz L M, Fontcuberta i Morral A and Johnston M B 2018 *Nano Lett.* **18** 3703–3710
[87] Pea M, Ercolani D, Li A, Gemmi M, Rossi F, Beltram F and Sorba L 2013 *J. Cryst. Growth* **366** 8–14
[88] Ercolani D, Gemmi M, Nasi L, Rossi F, Pea M, Li A, Salviati G, Beltram F and Sorba L 2012 *Nanotechnology* **23** 115606
[89] Heiss M, Ketterer B, Uccelli E, Morante J R, Arbiol J and i Morral A F 2011 *Nanotechnology* **22** 195601
[90] Lähnemann J, Hill M O, Herranz J, Marquardt O, Gao G, Al Hassan A, Davtyan A, Hruszkewycz S O, Holt M V, Huang C, Calvo-Almazán I, Jahn U, Pietsch U, Lauhon L J and Geelhaar L 2019 *Nano Lett.* **19** 4448–4457
[91] Herranz J, Corfdir P, Luna E, Jahn U, Lewis R B, Schrottke L, Lähnemann J, Tahraoui A, Trampert A, Brandt O and Geelhaar L 2020 *ACS Appl. Nano Mater.* **3** 165–174
[92] Buyanova I A and Chen W M 2019 *Nanotechnology* **30** 292002
[93] Wu J, Borg B M, Jacobsson D, Dick K A and Wernersson L E 2013 *J. Cryst. Growth* **383** 158–165
[94] Raya-Moreno M, Rurali R and Cartoixà X 2019 *Phys. Rev. Materials* **3**(8) 084607

$In_xGa_{1-x}As$		
T	x_m	x_M
100	0.40	0.70
300	0.35	0.70
500	0.35	0.70
$GaAs_{1-x}P_x$		
T	x_m	x_M
100	0.30	0.60
300	0.30	0.60
500	0.30	0.60
$InAs_{1-x}Sb_x$		
T	x_m	x_M
100	0.50	0.70
300	0.40	0.70
500	0.40	0.70
$GaAs_{1-x}N_x$		
T	x_m	x_M
100	0.40	0.60
300	0.20	0.50
500	0.20	0.50
$GaP_{1-x}N_x$		
T	x_m	x_M
100	0.30	0.60
300	0.15	0.40
500	0.15	0.40

Table 1: Lower (x_m) and upper (x_M) boundaries of the extreme alloying plateau.

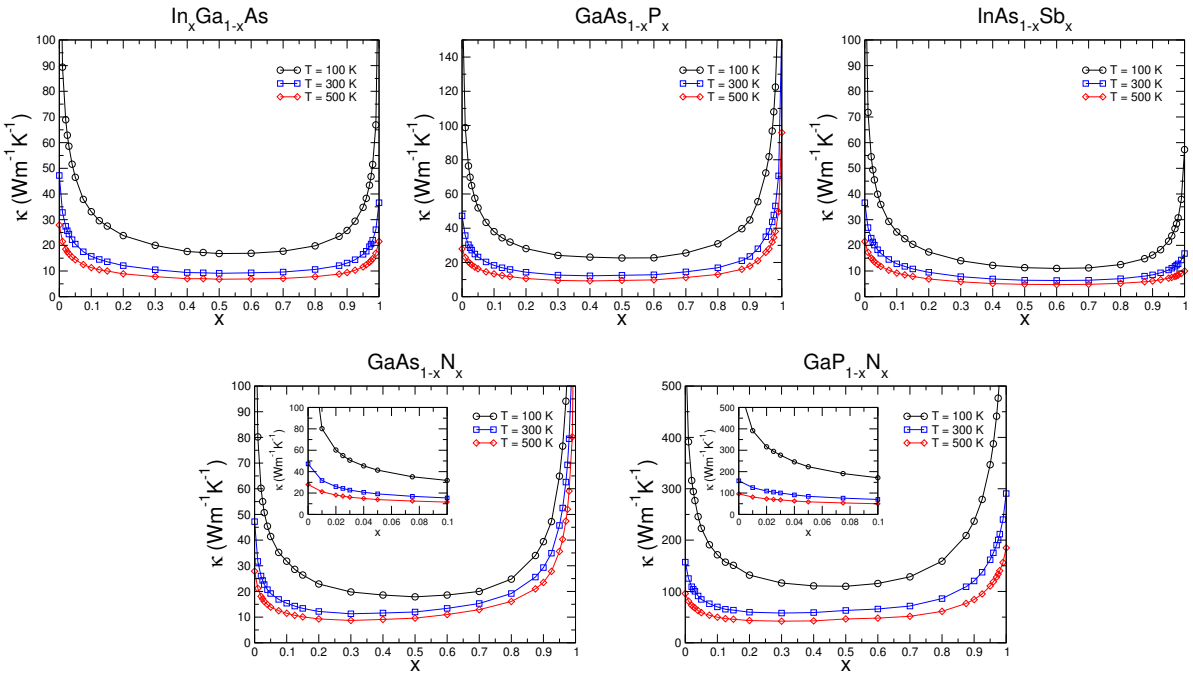

Figure 1: Thermal conductivity as a function of composition at T = 100, 300, and 500 K of $In_xGa_{1-x}As$, $GaAs_{1-x}P_x$, $InAs_{1-x}Sb_x$, $GaAs_{1-x}N_x$, $GaP_{1-x}N_x$. For the nitrides we display a magnified view of the low N content region.

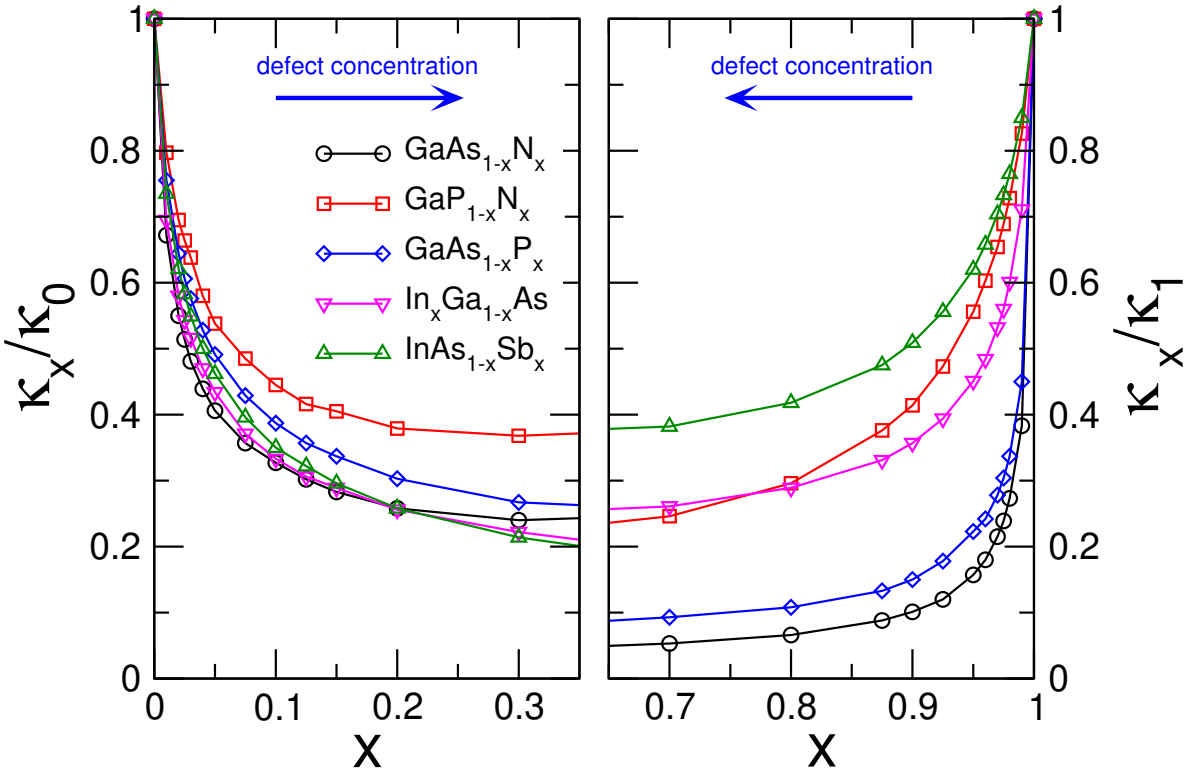

Figure 2: Reduction of the thermal conductivity as a function of alloying. Values are normalized to $\kappa(x = 0)$ for $x < 0.5$ and to $\kappa(x = 1)$ for $x > 0.5$ in order to focus on the effect of small quantities of a lattice impurity, e.g. In for GaAs (x close to 0) and Ga for InAs (x close to 1), in the case of $In_xGa_{1-x}As$; similarly for the other materials.

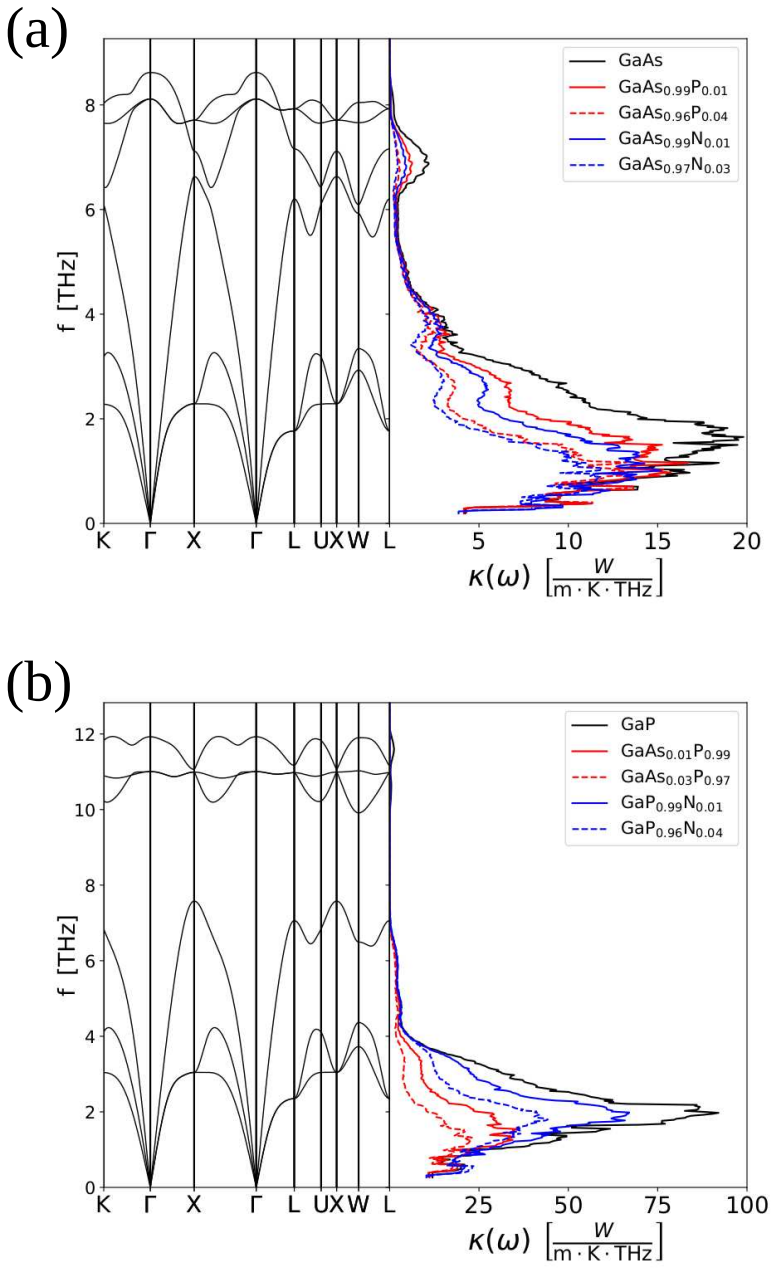

Figure 3: (a) Dispersion relation of GaAs and frequency resolved contributions to the thermal conductivity for GaAs, $GaAs_{1-x}P_x$ ($x = 0.01$ and $x = 0.04$), and $GaAs_{1-x}N_x$($x = 0.01$ and $x = 0.03$) at 300 K. (b) Dispersion relation of GaP and frequency resolved contributions to the thermal conductivity for GaP, $GaAs_{1-x}P_x$ ($x = 0.01$ and $x = 0.03$), and $GaP_{1-x}N_x$($x = 0.99$ and $x = 0.96$) at 300 K

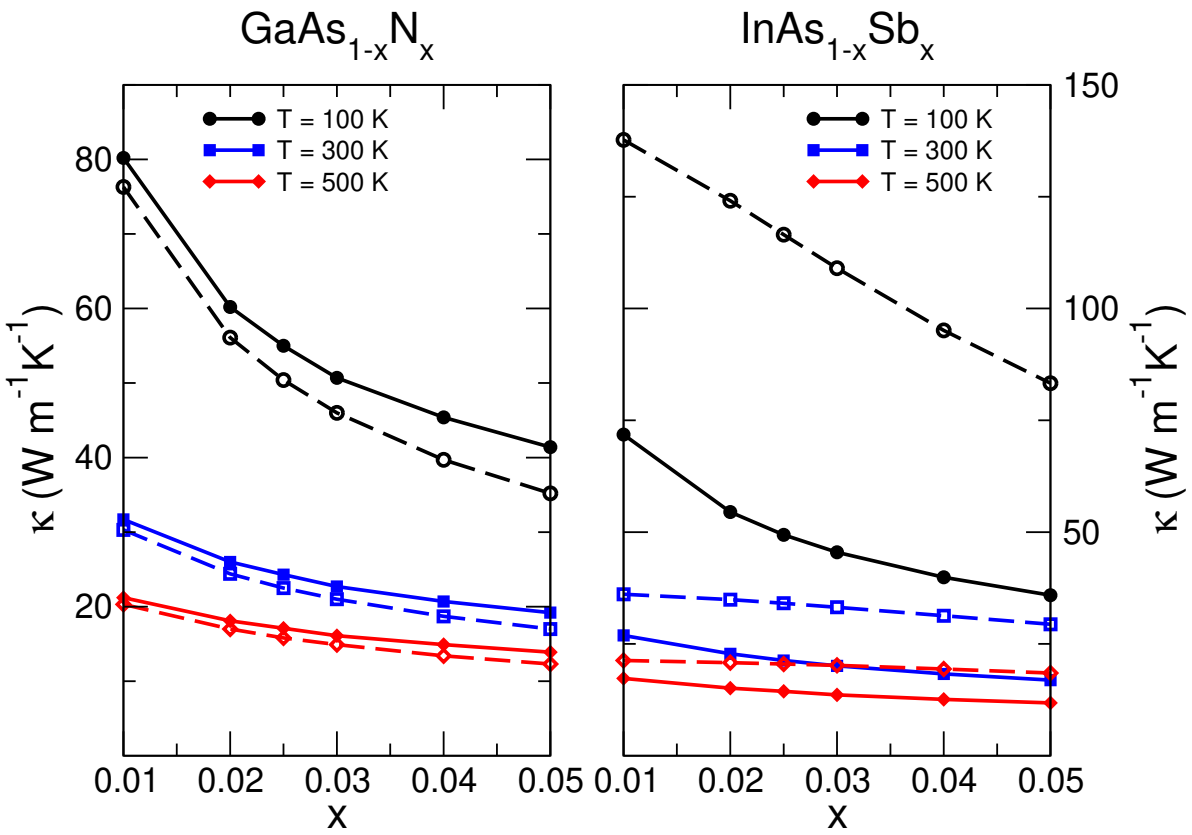

Figure 4: Thermal conductivity as a function of composition at $T = 100$, 300, and 500 K of $GaAs_{1-x}N_x$ and $InAs_{1-x}Sb_x$, as obtained from the virtual crystal, like in Fig. 1 (continuous lines) and within the mass defect model (dashed lines), where N and Sb are modeled as As atoms with the mass of N and Sb atoms, respectively.

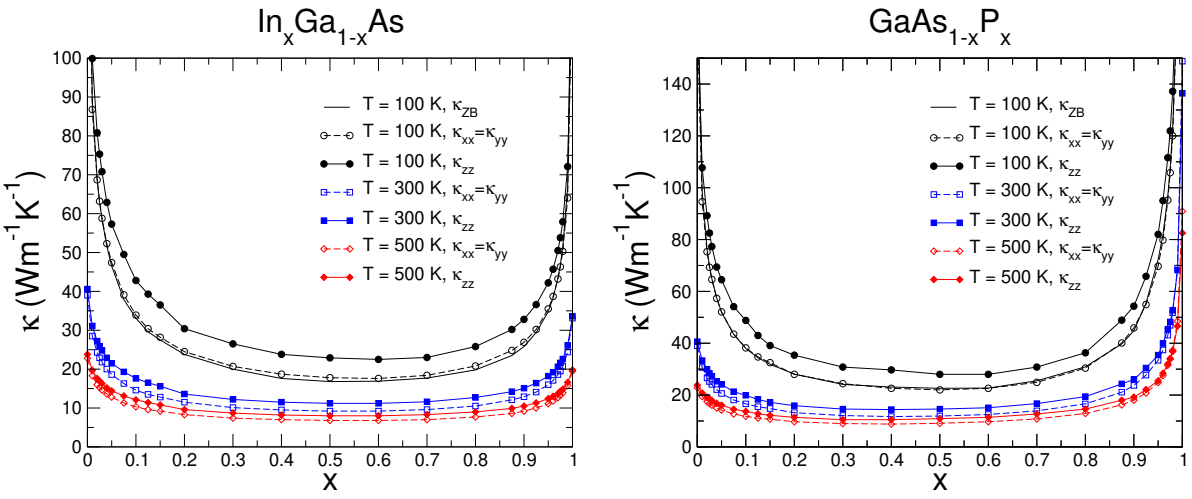

Figure 5: Thermal conductivity as a function of composition at T = 100, 300, and 500 K of wurtzite $In_xGa_{1-x}As$ and $GaAs_{1-x}P_x$. Empty symbols refer to $\kappa_{xx} = \kappa_{yy}$, while filled symbols refer to κ_{zz}.